Publisher's PDF, also known as Version of record

Link to published version (if available):
[10.1523/JNEUROSCI.1153-17.2017](#)

[Link to publication record in Explore Bristol Research](#)
PDF-document

University of Bristol - Explore Bristol Research
General rights

Cellular/Molecular

Cadherin-10 Maintains Excitatory/Inhibitory Ratio through Interactions with Synaptic Proteins

Katharine R. Smith,[1,5] Kelly A. Jones,[1] Katherine J. Kopeikina,[1] Alain C. Burette,[4] Bryan A. Copits,[3] Sehyoun Yoon,[1] Marc P. Forrest,[1] Jessica M. Fawcett-Patel,[1] Jonathan G. Hanley,[5] Richard J. Weinberg,[4] Geoffrey T. Swanson,[3] and Peter Penzes[1,2]

Departments of [1]Physiology, [2]Psychiatry and Behavioral Sciences, and [3]Pharmacology, Northwestern University Feinberg School of Medicine, Chicago, Illinois 60611, [4]Department of Cell Biology and Physiology, University of North Carolina, Chapel Hill, North Carolina 27599, and [5]Faculty of Biomedical Sciences, School of Biochemistry, University of Bristol, Bristol BS8 1TD, United Kingdom

Appropriate excitatory/inhibitory (E/I) balance is essential for normal cortical function and is altered in some psychiatric disorders, including autism spectrum disorders (ASDs). Cell-autonomous molecular mechanisms that control the balance of excitatory and inhibitory synapse function remain poorly understood; no proteins that regulate excitatory and inhibitory synapse strength in a coordinated reciprocal manner have been identified. Using super-resolution imaging, electrophysiology, and molecular manipulations, we show that cadherin-10, encoded by *CDH10* within the ASD risk locus 5p14.1, maintains both excitatory and inhibitory synaptic scaffold structure in cultured cortical neurons from rats of both sexes. Cadherin-10 localizes to both excitatory and inhibitory synapses in neocortex, where it is organized into nanoscale puncta that influence the size of their associated PSDs. Knockdown of cadherin-10 reduces excitatory but increases inhibitory synapse size and strength, altering the E/I ratio in cortical neurons. Furthermore, cadherin-10 exhibits differential participation in complexes with PSD-95 and gephyrin, which may underlie its role in maintaining the E/I ratio. Our data provide a new mechanism whereby a protein encoded by a common ASD risk factor controls E/I ratios by regulating excitatory and inhibitory synapses in opposing directions.

Key words: adhesion; cadherin-10; CDH10; dendritic spines; inhibitory synapses; PSD-95

Significance Statement

The correct balance between excitatory/inhibitory (E/I) is crucial for normal brain function and is altered in psychiatric disorders such as autism. However, the molecular mechanisms that underlie this balance remain elusive. To address this, we studied cadherin-10, an adhesion protein that is genetically linked to autism and understudied at the cellular level. Using a combination of advanced microscopy techniques and electrophysiology, we show that cadherin-10 forms nanoscale puncta at excitatory and inhibitory synapses, maintains excitatory and inhibitory synaptic structure, and is essential for maintaining the correct balance between excitation and inhibition in neuronal dendrites. These findings reveal a new mechanism by which E/I balance is controlled in neurons and may bear relevance to synaptic dysfunction in autism.

Introduction

The correct balance between excitation and inhibition (E/I balance) in neuronal circuits of the cerebral cortex is essential for effective information processing. At the cellular level, this balance is controlled by the number and strength of excitatory and inhibitory inputs. It has been proposed that disruption of synaptic E/I balance in the cortex underlies the pathology of some neuropsychiatric diseases, including autism spectrum disorders (ASDs; Gao and Penzes, 2015). To control neuronal excitability, individual neurons must maintain an appropriate ratio between excitatory and inhibitory inputs. Dysfunction of either excitatory or inhibitory synapses can shift this ratio, leading to pathological conditions, which suggests the presence of cellular mechanisms to

maintain a correct E/I ratio. However, the nature of these putative cell-autonomous molecular mechanisms that control E/I ratio in cortical neurons remain mostly unknown.

Numerous rare but highly penetrant point mutations have implicated synaptic adhesion molecules in controlling E/I balance. Whereas these rare variants have been extensively investigated (Betancur et al., 2009), they underlie only a small fraction of autism susceptibility. In contrast, common variants with small effect sizes have been estimated to account for >50% of autism susceptibility (Klei et al., 2012; Gaugler et al., 2014), although their neurobiology is far less studied. The function of common variants may, therefore, provide crucial insights into ASD pathogenesis. The first genome-wide association study finding common variants for ASD revealed strong association signals with single nucleotide polymorphisms between the genes encoding cadherin-9 and cadherin-10 (*CDH9* and *CDH10*; Wang et al., 2009), a finding replicated in additional studies (Ma et al., 2009; Prandini et al., 2012; Connolly et al., 2013). Cadherin-9 is highly expressed in hippocampus where it is required for formation of dentate gyrus–CA3 synapses (Williams et al., 2011). In contrast, cadherin-10 is highly expressed in the neocortex (Bekirov et al., 2002; Gil et al., 2002; Wang et al., 2009), including frontal regions relevant for ASD, but remains uncharacterized at the cellular level.

Classical cadherins are single-pass transmembrane glycoproteins with a cytoplasmic domain that mediates downstream signaling and a large extracellular domain that engages in homophilic and heterophilic adhesion. The classical cadherin family includes type I cadherins, exemplified by N-cadherin and E-cadherin, and type II cadherins, including cadherin-6, -8, -9, and -10. Type I cadherins have a broad tissue distribution, whereas type II cadherins are restricted to specific brain regions or circuits (Suzuki et al., 1997). Research to date has focused on type I cadherins. Recent studies have identified diverse functions for type II cadherins in cerebellar, retinal, and hippocampal circuits (Williams et al., 2011; Duan et al., 2014; Kuwako et al., 2014), but very little is yet known about the function(s) of type II cadherins in cerebral cortex.

Here, we show that cadherin-10 is important for maintaining the balance between excitatory and inhibitory synapse function in cortical neurons. Using immunogold-electron microscopy (EM) and super-resolution microscopy, we demonstrate that cadherin-10 is distributed at both excitatory and inhibitory synapses as nanoscale puncta, the number and position of which correlate with PSD size. Reducing levels of cadherin-10 exerts complementary effects on excitatory and inhibitory synapse size and function, leading to reduced excitation and increased inhibition. Cadherin-10 mediates these effects via participation in complexes with PSD-95 and gephyrin. Together, our data suggest a new mechanism whereby a protein encoded by a common risk locus for ASD maintains appropriate E/I ratio by reciprocal actions on excitatory and inhibitory synapses.

Materials and Methods

Antibodies. The following antibodies were purchased: mouse anti-PSD-95 monoclonal (RRID:AB_2292909; Neuromab), mouse anti-GFP monoclonal (RRID:AB_1587098; Millipore), chicken anti-GFP polyclonal (RRID:AB_300798; Abcam), mouse anti-myc monoclonal (University of Iowa Hybridoma Bank and RRID:AB_627266; Santa Cruz Biotechnology), rabbit anti-cadherin-10 polyclonal (T2, to the C terminus, RRID:AB_2275951; Santa Cruz Biotechnology), mouse anti-turboGFP (RRID:AB_2622256; Origene), rabbit anti-α2 GABA$_A$R (RRID:AB_2108839; Synaptic Systems), mouse anti-gephyrin (RRID: AB_887716 for immunocytochemistry, RRID:AB_887719 for Western blot; Synaptic Systems), anti-synaptophysin antibody (RRID:AB_477523;

Sigma-Aldrich), rabbit anti-GluA1 (RRID:AB_1977216; Millipore), mouse anti-β3-GABA$_A$R (RRID:AB_2109585; Neuromab), mouse anti-NL2 (RRID:AB_993011; Synaptic Systems), mouse anti-NL1 (RRID: AB_2235964; Neuromab), mouse anti-Caspr2 (RRID:AB_2245198; Neuromab), anti-N-cadherin (RRID:AB_398236; BD Biosciences). Goat anti-mouse IgG, anti-rabbit IgG, or anti-chicken IgG antibodies conjugated with Alexa Fluor 488 (RRID:AB_143165, RRID:AB_143160, and RRID:AB_142924) or Alexa Fluor 568 (RRID:AB_144696 and RRID: AB_141416; Invitrogen) were used as secondary antibodies in immunostaining experiments. Horseradish peroxidase-conjugated anti-mouse IgG (RRID:AB_228307) and anti-rabbit IgG (RRID:AB_228341) antibodies (Thermo Fisher Scientific) were used as secondary antibodies in Western blotting experiments.

Plasmids. Myc-tagged cadherin-10 and small hairpin RNA (shRNA) constructs against cadherin-10 were purchased from Origene (RRID: SCR_008985). The shRNA targeted nucleotides 384–413 of the cadherin-10 open reading frame (NCBI Reference Sequence: NM_009865.2). The shRNA was expressed under the U6 promoter in pGFP-V-RS (Origene; RRID: SCR_008985). A turbo-GFP gene under a CMV promoter was expressed from the same plasmid to enable identification of transfected cells. The control is a scrambled target sequence, purchased from Origene. The RNAi-resistant myc-cadherin-10 construct was produced using the Quick Change mutagenesis protocol.

Cortical slice preparation and imaging. Male Sprague Dawley rats were deeply anesthetized with sodium pentobarbital (60 mg/kg, i.p.) and intracardially perfused with 4% paraformaldehyde (PFA) in phosphate buffer (PB; 0.1 M, pH 6.8) for light microscopy or a mixture of 2% PFA and 2% glutaraldehyde in PB for EM. Brains were then removed and postfixed for 2 h in the same fixative. Brains were cut at 40 and 100 μm on a vibratome. Forty-micrometer free-floating sections were incubated in 10% normal donkey serum and then in primary antibody, followed by donkey IgG conjugated to DyLight 488 and DyLight 549. Slices were imaged using a Leica SP2 microscope, and 36 single-plane high-resolution fields (20 × 20 μm) from three rats were analyzed using Velocity software.

EM and analysis. One hundred-micrometer sections were pretreated in 0.1% calcium chloride in 0.1 M sodium acetate, rinsed, and cryoprotected in a graded series to 30% glycerol in 0.1 M sodium acetate. Sections were quick-frozen in methanol chilled with dry ice. Freeze substitution in 4% uranyl acetate in methanol was performed in a Leica Electron Microscopy Automatic Freeze Substitution System; after rinsing in methanol, sections were infiltrated with Lowicryl HM-20, mounted between sheets of ACLAR supported by pieces of glass slice, and polymerized with ultraviolet light.

Sections were glued to plastic blocks, cut at ∼70–90 nm with an ultramicrotome and collected on nickel grids. Grids were pretreated 15 min at 60°C in 0.01 M citrate buffer, pH6, rinsed in water, blocked in 1% BSA in Tris-buffered saline with 0.005% Tergitol NP-10, and incubated overnight at 21–24°C with the primary antibodies. Grids were rinsed, blocked in 1% normal goat serum, and incubated in secondary antibodies for 2 h (for single labeling: goat antibody to rabbit IgG F(ab)2 conjugated to 10 nm gold particles; for double labeling: goat antibody to rabbit IgG F(ab)2 conjugated to 20 nm gold particles and goat antibody to mouse IgG F(ab)2 conjugated to 10 nm gold particles; Ted Pella). Grids were then rinsed and counterstained with 1% uranyl acetate, followed by Sato's lead. Electron microscopy was performed with a Philips Tecnai electron microscope at 80 kV with a magnification at 10,000–40,000×; images were acquired with a Gatan 12-bit 1,024 × 1,024 CCD camera. Random grid squares were chosen, and image acquisition was done with the observer blind to the study. Synapses were analyzed if they were asymmetric and had well defined membranes, postsynaptic densities, and presynaptic terminals with synaptic vesicles. Positions of gold particles were measured using ImageJ (National Institutes of Health; RRID:SCR_003070); data were analyzed using Kaleidograph software.

Neuronal cell culture and transfection. Dissociated cultures of primary cortical neurons were prepared from E18 Sprague Dawley rat embryos of either sex, as previously described (Smith et al., 2014). Briefly, brains were dissected in ice-cold HBSS, and cortical tissue was isolated, digested with papain [Sigma; diluted in Neurobasal with EDTA (0.5 mM) and DNaseI (2 units/ml), activated with L-cysteine (1 mM) at 37°C], and

mechanically dissociated in neuronal feeding medium [Neurobasal plus B27 supplement (Invitrogen) plus 0.5 mM glutamine plus penicillin/streptomycin]. Neurons were plated on coverslips previously coated with poly-D-lysine (0.2 mg/ml; Sigma), at 300,000 cells per coverslip in neuronal feeding medium. One hour after seeding, medium was replaced. Neuronal cultures were maintained at 37°C in 5% CO_2. Neuronal feeding medium was supplemented with 200 μM D,L-amino-phosphonovalerate (Ascent Scientific) beginning on DIV 4. For transfection, plasmids (1–10 μg total DNA) and Lipofectamine 2000 (Invitrogen) were diluted in DMEM plus HEPES (10 mM), mixed thoroughly together, and incubated for 20–30 min at 37°C before adding to cultured neurons. After transfection, antibiotic containing feeding medium containing half-conditioned and half-fresh medium was added to the cultures, and the constructs were expressed for 3 d or as indicated.

HEK293 cell transfection. HEK293 cells were maintained in DMEM (Invitrogen), supplemented with 10% heat-inactivated fetal bovine serum and penicillin–streptomycin, and transfected by Lipofectamine 2000 as described above. Plasmids were expressed for 48 h and harvested in pull-down buffer [50 mM Tris, pH 7.5, 1% Triton X-100, 150 mM NaCl, with protease inhibitor cocktail (Roche)] for SDS-PAGE and Western blotting.

Immunocytochemistry. Neurons were fixed for 10 min in 4% formaldehyde/4% sucrose in PBS and then at 4°C in methanol prechilled to −20°C for 10 min. Fixed neurons were permeabilized and blocked simultaneously in PBS containing 2% normal goat serum and 0.2% Triton X-100 for 1 h at room temperature. Primary antibodies were added in PBS containing 2% normal goat serum overnight at 4°C, followed by three 10 min washes in PBS. Secondary antibodies were incubated for 1 h at room temperature, also in 2% normal goat serum in PBS. Three additional washes (15 min each) were performed before coverslips were mounted using ProLong antifade reagent (Invitrogen).

Confocal microscopy. Confocal images of immunostained neurons were obtained with a Ziess LSM5 Pascal confocal microscope. Images were taken using the 63× oil-immersion objective (NA 1.4) collecting a z-series of 5–10 images, averaged two times, and taken at 0.37 μm intervals with 1024 × 1024 pixel resolution. Detector gain and offset were adjusted in the channel of cell fill (GFP) to include all spines and to enhance edge detection.

Dendritic spine quantification. Two-dimensional, background-subtracted maximum projection reconstructions of images for dendritic spine morphometric analysis (area, length, and width) and quantification of spine linear density (number of spines/10 μm dendritic length) were performed using MetaMorph software (Molecular Devices) as described previously (Smith et al., 2014). Briefly, a threshold was applied to the maximum projection images to include all detectable spines, and regions along dendrites containing dendritic spines were manually traced to enclose spines but not the dendritic shaft or other structures. Dendritic spine "objects," restricted to objects with areas >0.1 μm^2, were automatically detected by MetaMorph, and the area, maximum length, and head width of each spine were measured. Two dendritic branches ($\sim$100 μm) of each neuron were analyzed. Only spines on secondary and tertiary apical dendrites were measured to reduce variability. Cultures that were directly compared were stained simultaneously and imaged with the same acquisition parameters. For each condition, 3–10 neurons each from three to five separate experiments were used. Experiments were performed blind to conditions and on sister cultures.

Confocal image analysis. Colocalization of synaptic proteins (PSD-95 and gephyrin) with cadherin-10 was quantified using MetaMorph. Background-subtracted images were thresholded, regions along dendrites were outlined, and total immunofluorescence intensity for each cluster was measured automatically. To determine the degree of colocalization between two channels, each channel was thresholded to select distinct puncta as described above. A 100 μm dendritic region was selected, and puncta counts were made; puncta smaller than 0.065 μm^2 were excluded from analysis. Regions representing the measured puncta in one channel were generated using MetaMorph and overlaid onto the other channel. Puncta were counted as colocalized (positive) if the average intensity within the overlaid region exceeded threshold. Thresholds

were set individually for each antibody and held constant across all images.

Structured illumination microscopy. Multichannel structured illumination microscopy (SIM) images were acquired as described by Smith et al. (2014), using a Nikon Structured Illumination super-resolution microscope with 100× (NA 1.4) objective. During acquisition, auto-exposure was kept between 100 and 300 ms and laser power was adjusted to keep Lookup tables (LUTs) within the first quarter of the scale ($<$4000). Z-stacks ($z = 0.2$ μm, seven to eight slices) were reconstructed using Nikon Elements software. Three reconstruction parameters (Illumination Modulation Contrast, High Resolution Noise Suppression, and Out of Focus Blur Suppression) were extensively tested to generate consistent images across experiments without abnormal features or artifacts and producing the best Fourier transforms. Reconstruction parameters (0.96, 1.19, and 0.17) were kept consistent across experiments and imaging sessions. Resolution of images was confirmed with full-width halfmaximum (FWHM) measurements of a small structure within the image.

SIM analysis. Images were processed and analyzed using Nikon Elements software (RRID:SCR_014329), MetaMorph (RRID:SCR_002368), and ImageJ and displayed as maximum projections. Single PSD-95 and gephyrin analyses were performed on $\sim$180 PSDs across four to five neurons per condition using Nikon Elements or ImageJ software. PSD-95, gephyrin, and cadherin-10 diameters were assessed as the FWHM and measured in ImageJ with a line scan across the maximum width of the cluster. Gaussian fits of these intensity profiles were performed in GraphPad Prism, and the FWHM was calculated. Visual assessment of fluorescence intensity was used to delineate separate or connected puncta. We only took into account the position of cadherin-10 puncta that touched or overlapped with synaptic staining (i.e., both perisynaptic and central that touched the synaptic cluster). A cadherin-10 punctum that was touching or overlapping with a gephyrin or PSD-95 puncta was included in the analyses. This was achieved by visual assessment of fluorescence intensity between the cadherin-10 punctum and the PSD. Puncta were considered separate if a region of decreased intensity was readily visible between the puncta and the PSD. This approach was then confirmed with the Nikon Elements automated detection software and kept consistent throughout all analyses. The number of cadherin-10 puncta associated with the PSD was quantified manually and recorded. Based on the localization of cadherin-10 with respect to the PSD, synapses were classified into one of three groups. The central group included synapses with cadherin-10 puncta entirely enveloped by the PSD and not touching the edge of the PSD. The perisynaptic group contained synapses that harbored cadherin-10 puncta that were confined to and touching the edge of the PSD. The central/perisynaptic group contained synapses that had at least one cadherin-10 punctum that was perisynaptic, and one cadherin-10 punctum that was central.

Electrophysiology. Cultured cortical neurons were recorded in wholecell configuration 3 d after transfection (DIV 24) as described previously (Smith et al., 2014). The extracellular solution contained 140 mM NaCl, 10 mM glucose, 10 mM HEPES, 3 mM KCl, 2 mM $CaCl_2$, and 1 mM $MgCl_2$, pH 7.3. Patch pipettes were pulled from borosilicate glass and firepolished to a resistance of 3–5 MΩ. The intracellular patch-pipette solution contained 95 mM CsF, 25 mM CsCl, 10 mM HEPES, 10 mM EGTA, 2 mM NaCl, 2 mM Mg-ATP, 10 mM QX-314, 5 mM tetraethylammonium chloride, and 5 mM 4-amino- pyridine, pH 7.2. Neurons were voltage clamped at −70 mV, and currents were recorded using pClamp9 software with an Axopatch 200B amplifier (Molecular Devices). Miniature EPSCs (mEPSCs) were isolated by bath application of 10 μM bicuculline, 50 μM picrotoxin, 50 μM D,L-aminophos-phonovalerate, and 1 μM tetrodotoxin. Verification that mEPSCs were mediated by AMPA receptors was achieved by adding 50 μM CNQX at the end of recordings. Miniature IPSCs (mIPSCs) were isolated by the addition of APV (50 μM) and CNQX (20 μM). Recordings were filtered at 5 kHz and digitized at 20 kHz. The data were low-pass filtered using a 1 kHz cutoff and analyzed blind to condition with Mini-Analysis software (Synaptosoft).

Coimmunoprecipitation assays. DIV 20–22 cortical neurons or homogenized rat cortex were solubilized for 1 h in pull-down buffer [50 mM Tris, pH 7.5, 1% Triton X-100, 150 mM NaCl, with protease inhibitor
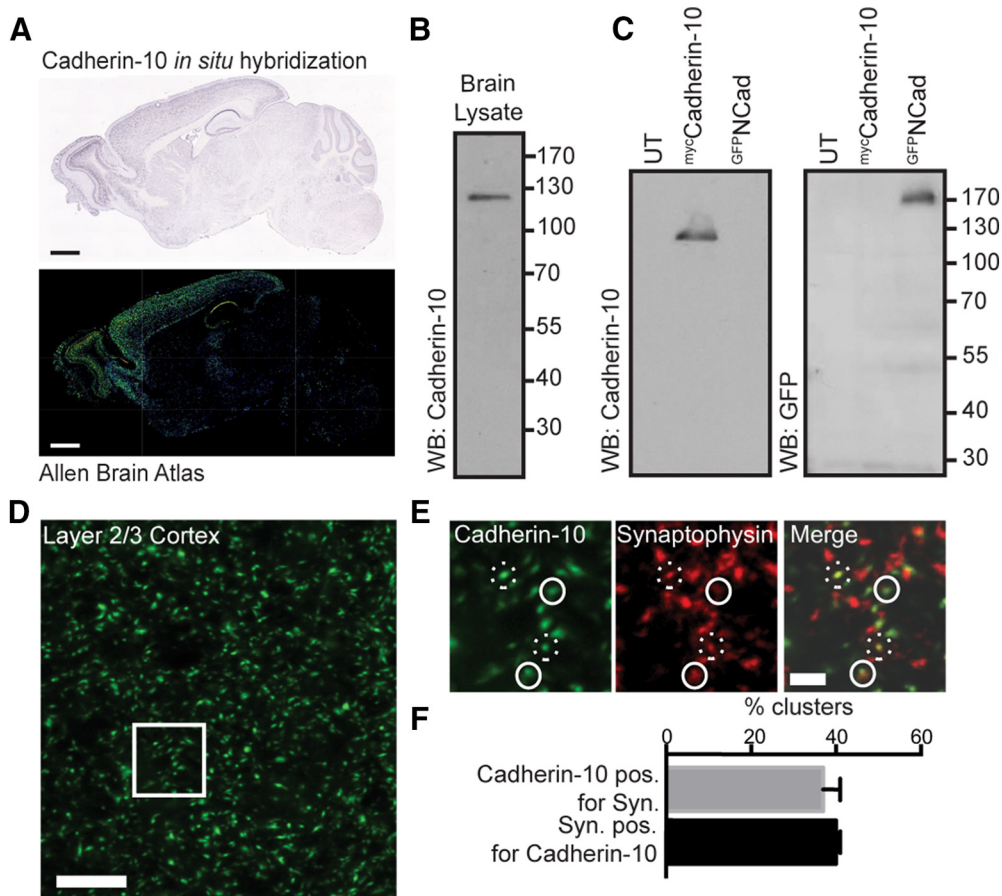
Figure 1. Expression and distribution of cadherin-10 in cortex. *A*, *In situ* hybridization of cadherin-10, reproduced from the Allen Brain Atlas database showing high expression of cadherin-10 in cerebral cortex and CA1 region of hippocampus. Scale bars, 1 mm. *B*, Representative Western blot (WB) of whole brain lysate, probed with cadherin-10 antibody ($n = 4$ independent experiments). *C*, Representative WB of lysates from HEK293 cells expressing ^{myc}cadherin-10, ^{GFP}N-cadherin, or untransfected control (UT). Blots are probed with antibodies to cadherin-10 or GFP ($n = 3$ independent experiments). *D*, Light microscopy image of layer 2/3 of cerebral cortex immunostained for cadherin-10. Scale bar, 10 μm. *E*, Enlargement of the boxed region in *D*, immunostained for cadherin-10 (green) and synaptophysin (red); closely apposed puncta are marked with solid white circles and overlapping puncta with dotted circles. Scale bar, 2 μm. *F*, Quantification of cadherin-10 and synaptophysin (Syn.) colocalization showing $37 \pm 5\%$ of cadherin-10 clusters were positive (pos.) for synaptophysin and $40 \pm 2\%$ synaptophysin clusters were positive for cadherin-10.

cocktail (Roche)]. Solubilized material was centrifuged at $16,000 \times g$ for 10 min at 4°C, and the supernatant was precleared with protein G beads for 1 h. Proteins were immunoprecipitated with 2 μg of cadherin-10 antibody for 2 h, followed by a 1 h incubation with protein G beads. Beads were then washed four times, and bound complexes were analyzed by SDS-PAGE and Western blotting.

Membrane fractionation. Cortices from 6-week-old mice were homogenized in sucrose buffer (20 mM HEPES, pH 7.4, 320 mM sucrose, and 5 mM EDTA) supplemented with protease inhibitor cocktail (Roche). Homogenates were centrifuged at low speed to pellet nuclei and cell debris ($3000 \times g$ for 20 min at 4°C), and the supernatant (S1) was then centrifuged at high speed ($38,000 \times g$ for 30 min at 4°C) to obtain a membrane pellet (P2). P2 was resuspended in potassium iodide buffer (20 mM HEPES, pH 7.4, 1 M KI, and 5 mM EDTA) to remove membrane-associated proteins (S3), and membranes were again collected by centrifugation ($38,000 \times g$ for 20 min at 4°C). Membranes were washed (20 mM HEPES, pH 7.4, and 5 mM EDTA) and pelleted once more (S4) before solubilizing in CHAPS buffer supplemented with protease inhibitors (20 mM HEPES, pH 7.4, 100 mM NaCl, 5 mM EDTA, and 1% CHAPS) for 2 h at 4°C. Solubilized membranes were clarified by centrifugation for 30 min at $100,000 \times g$ at 4°C (S5). The final CHAPS-insoluble pellet was resuspended in SDS buffer (50 mM Tris, pH 7.4, 150 mM NaCl, and 1% SDS) supplemented with protease inhibitors, solubilized at 37°C for 20 min, and clarified by centrifugation (S6).

Experimental design and statistical analysis. N numbers refer to the number of cells per condition unless otherwise stated. All experiments

were performed at least three times from three separate neuron cultures. All statistical tests were performed with GraphPad Prism. Data were tested for normality with D'Agostino and Pearson's tests to determine use of nonparametric (Mann–Whitney test, Kruskal–Wallis test, Spearman's correlation) or parametric (*t* test, ANOVA, Pearson's correlation) tests, as described in the text. Comparisons between two sets of data were performed with an unpaired *t* test. Data with three or more groups were analyzed by one-way ANOVA, followed by Bonferroni's *post hoc* comparison. Spearman's or Pearson's correlation was used to evaluate correlations between numbers of cadherin-10 puncta and PSD-95 or gephyrin cluster diameters. Two-way ANOVA was used to analyze differences in the distribution of cadherin-10 puncta relative to gephyrin and PSD-95 clusters, followed by a Bonferroni's *post hoc* comparison. *P* values were considered significant if less than 0.05. Bar graphs are displayed as mean $\pm$ SEM, unless otherwise noted.

Results

Expression and distribution of cadherin-10 in cortex

Cadherin-10 is reported to be enriched in frontal cortex and the CA1 region of the hippocampus (Bekirov et al., 2002; Gil et al., 2002; Wang et al., 2009; Fig. 1A), although its precise cellular localization and function in these regions remains unknown. To study its expression, we used a cadherin-10 antibody, which identifies a single band at the correct molecular weight by Western blotting of rat brain lysate and recognizes exogenously expressed
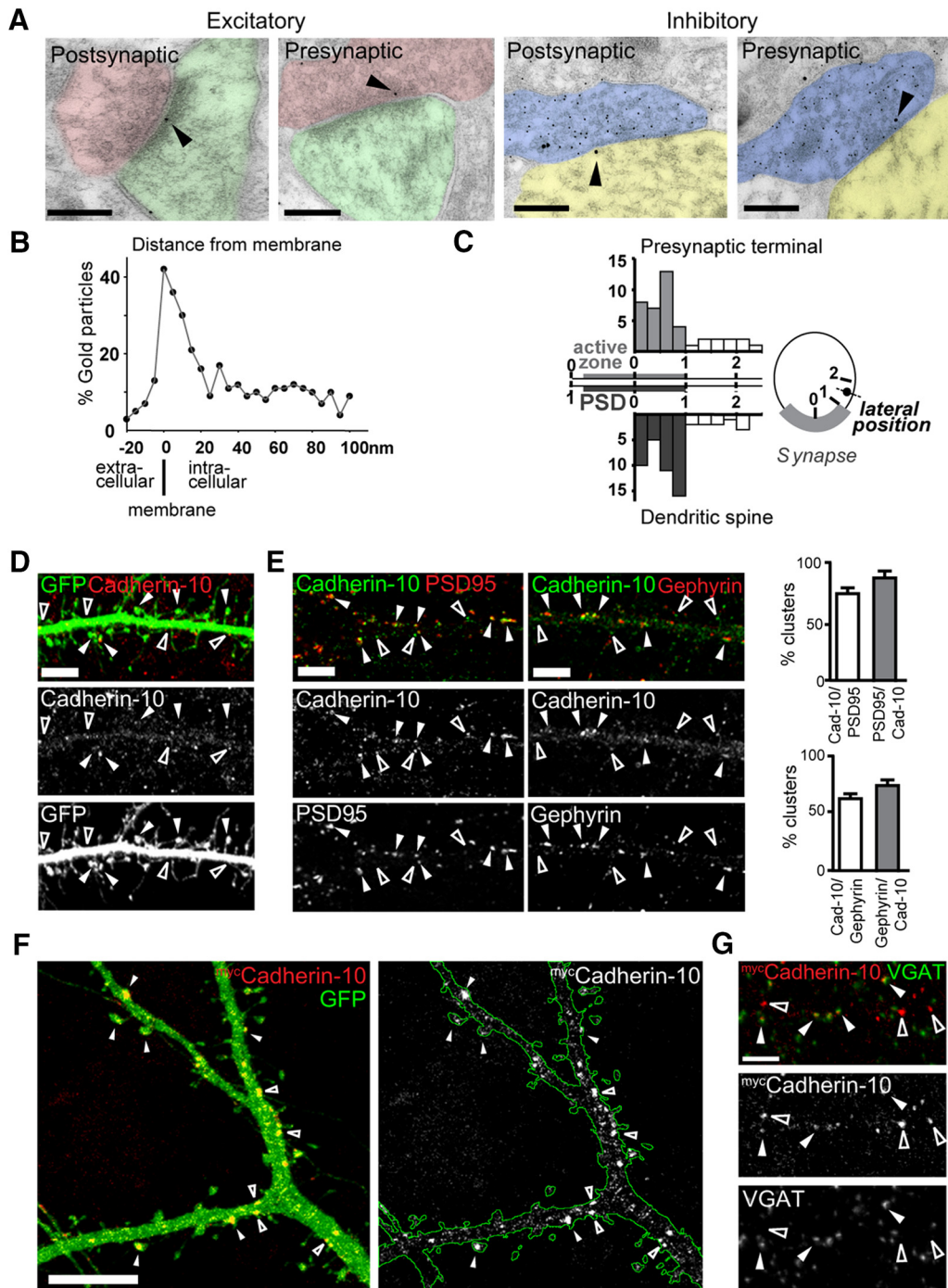
Figure 2. Cadherin-10 is localized to excitatory and inhibitory presynaptic and postsynaptic sites. **A**, Immunogold-EM micrographs of excitatory and inhibitory synapses from layer 2/3 of neocortex. A glutamatergic terminal is colorized in pink, a postsynaptic spine in green, a GABAergic terminal in blue, and opposing postsynaptic dendrites in yellow. Large dots are gold particles coding for cadherin-10, and small dots code for GABA. Arrowheads point to cadherin-10 immunoreactivity. Scale bars, 200 nm. **B, C**, Quantitative analysis of cadherin-10 gold particle position relative to the postsynaptic plasma membrane in the perpendicular axis (**B**) and lateral position tangentially along the plasma membrane (**C**; position 0, central; position 1, perisynaptic; position 2, extrasynaptic; 100 synapses from 4 rats). **D**, Confocal image of DIV 21 cortical dendrite expressing GFP and immunostained with antibodies to cadherin-10. Scale bar, 5 μm. Arrowheads point to cadherin-10 in spines, and open arrowheads point to cadherin-10 in the dendritic shaft. **E**, Confocal images of DIV 21 cortical dendrites immunostained with antibodies to cadherin-10 PSD-95 (left) and gephyrin (right); bar graphs quantify the percentage of cadherin-10 (Cad-10) clusters that colocalize with synaptic marker clusters. Scale bars, 5 μm. **F**, Confocal image of cortical neuron expressing [myc]cadherin-10 and GFP. Filled arrowheads point to cadherin-10 puncta in spines, and open arrowheads point to cadherin-10 in the dendritic shaft. Scale bar, 5 μm. **G**, Confocal image of cortical neuron expressing [myc]cadherin-10 and immunostained with antibodies to vesicular GABA transporter to identify GABAergic terminals.

cadherin-10 but does not recognize exogenously expressed N-cadherin (Fig. 1B,C). We labeled histological sections from adult rat forebrain with antibodies to cadherin-10 and the presynaptic marker synaptophysin, focusing our attention on layer 2/3. Cadherin-10 was organized into numerous puncta throughout the neuropil (Fig. 1D): ~40% were colocalized with synaptophysin clusters (Fig. 1E), suggesting association of cadherin-10 with synaptic sites.
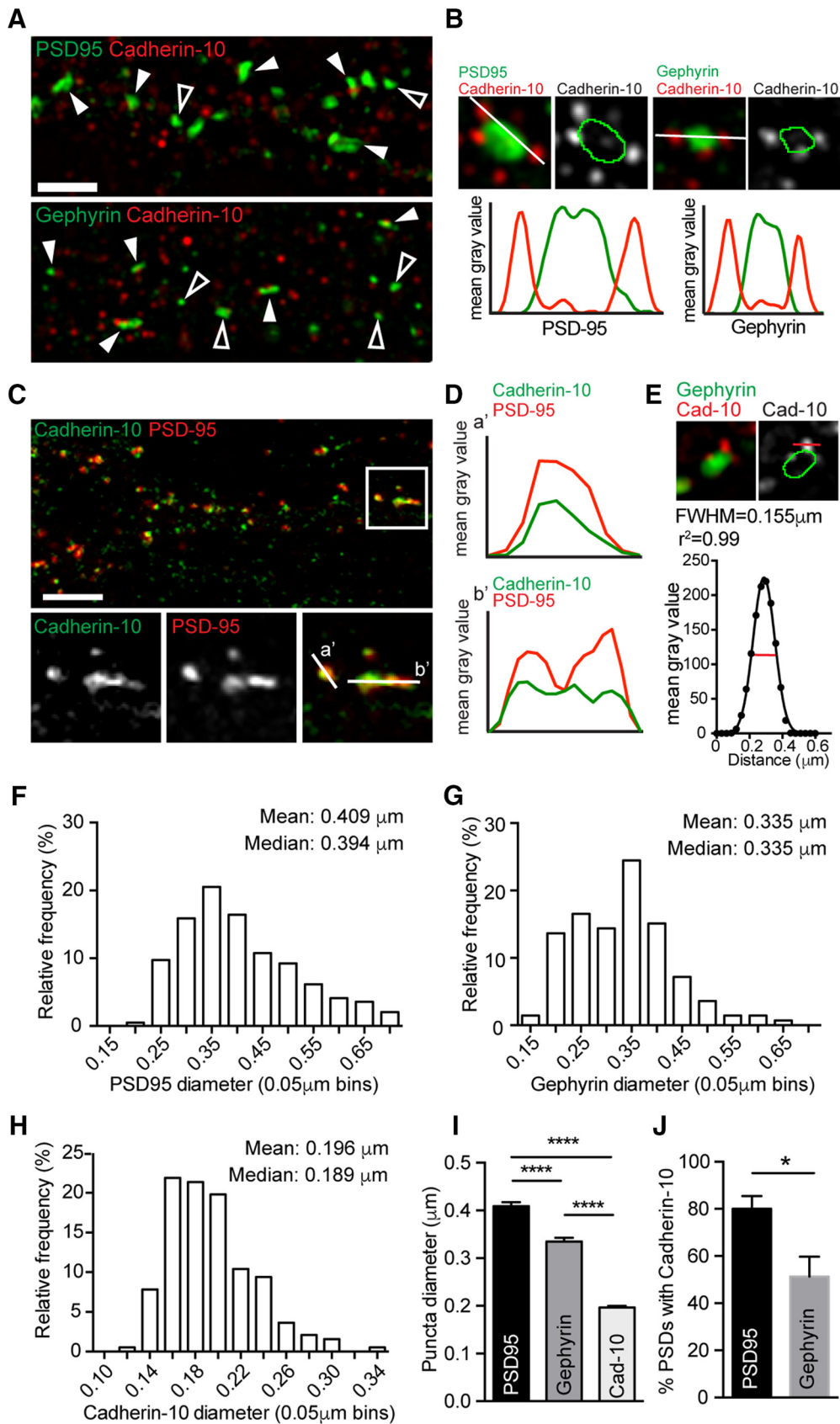
Figure 3. Cadherin-10 forms nanoscale puncta at cortical synapses *A*, SIM images of cortical dendrites immunostained for cadherin-10 and PSD-95 or gephyrin (maximum projections of z-stacks). Filled arrowheads point to cadherin-10-positive clusters, and open arrowheads point to cadherin-10-negative clusters. Scale bar, 2 μm. *B*, High-magnification views of cadherin-10 puncta at PSD-95 and gephyrin clusters. White lines show the path of line scans represented in the graphs below the images. *C, D*, Confocal image of a DIV 24 cortical neuron immunostained for cadherin-10 and PSD-95 (scale bar, 5 μm; maximum projection of z-stack). The boxed region is shown at higher magnification below. White lines (a′ and b′) produced line scans in *D* showing similar cluster diameter for cadherin-10 and PSD-95 when imaged by confocal microscopy. *E*, Top, High-magnification SIM image showing the small cadherin-10 cluster lies (*Figure legend continues.*)

Cadherin-10 is localized to excitatory and inhibitory presynaptic and postsynaptic sites

Cadherin-10 displays homophilic adhesion (Shimoyama et al., 2000), suggesting that postsynaptic cadherin-10 might interact with a presynaptic pool of cadherin-10 to mediate adhesion at synapses. To assess presynaptic versus postsynaptic location of cadherin-10, we performed immunogold-EM, which showed cadherin-10 labeling was both at the presynaptic active zone and the PSD of excitatory synapses (Fig. 2A). Double labeling for the inhibitory neurotransmitter GABA revealed that cadherin-10 gold particles were also present presynaptically and postsynaptically at inhibitory synapses. Quantitative analysis of gold-particle-labeled cadherin-10 in cortex (from four rats, 25 synapses per rat) showed that ~48% of gold particles lay within 20 nm of the membrane (Fig. 2B). Further analysis of the lateral position of gold particles along the plasma membrane showed that membrane-associated cadherin-10 was strongly associated with the synaptic specialization, both at the presynaptic and postsynaptic sites (Fig. 2C). Indeed, the presence of cadherin-10-labeled gold particles was ~12-fold higher within the synapse (central and perisynaptic positions 0 and 1) compared with extrasynaptic regions (position 2). Together, these data support both presynaptic and postsynaptic localization for cadherin-10 at both excitatory and inhibitory synapses in layer 2/3 cortex.

We then wanted an *in vitro* system to facilitate experimental manipulation, but first we verified that cadherin-10 displayed the same pattern of synaptic localization as shown in the intact brain. Using confocal microscopy, to allow good spatial separation of synapses, we characterized the localization of cadherin-10 in a mature low-density cortical culture system. Cadherin-10 appeared as discrete puncta throughout the dendritic tree, distributed both along the dendritic shaft and in dendritic spines, as demonstrated by labeling of GFP-filled neurons (Fig. 2D). Cadherin-10 was present at both PSD-95 and gephyrin-positive clusters, confirming localization at excitatory and inhibitory synapses (Fig. 2E). Furthermore, exogenous myc-tagged cadherin-10 was expressed in dendritic spines (the main locus of excitatory synapses) and colocalized with the inhibitory synaptic marker vesicular GABA transporter (Fig. 2F,G), confirming that postsynaptic cadherin-10 is localized at both types of synapses. Together, these data place cadherin-10 in an ideal position to modulate both excitatory and inhibitory synaptic adhesion and, hence, excitatory and inhibitory synapse function.

Super-resolution imaging of cadherin-10 at synapses

Super-resolution microscopy offers a new window into the nanoscale organization of synaptic proteins (Frost et al., 2010; MacGillavry et al., 2013; Nair et al., 2013; Lu et al., 2014; Smith et al., 2014). SIM (Gustafsson, 2005; Smith et al., 2014) enabled us to determine the subsynaptic distribution of cadherin-10 at excitatory and inhibitory synapses over a broader field of view and with higher immunocytochemical sensitivity than offered by

←
_____

(*Figure legend continued.*) adjacent to the large gephyrin cluster. To analyze the cadherin-10 puncta diameter, we generated a line scan (right, red line). Bottom, Gaussian fit of pixel-intensity profile across the cadherin-10 cluster. FWHM of profile was used to determine cluster diameter. *F*, *H*, Frequency distributions of PSD-95 (*F*), gephyrin (*G*), and cadherin-10 (*H*) cluster diameter. *I*, Mean diameter of PSD-95, gephyrin, and cadherin-10 clusters; PSD-95, 0.409 ± 0.009 μm; gephyrin, 0.335 ± 0.008 μm; cadherin-10, 0.196 ± 0.003 μm; ****p = 0.0001, Kruskal–Wallis test; n = 132–195 PSDs. *J*, Percentages of cadherin-10-positive PSD-95 and gephyrin clusters (PSD-95, 80.6 ± 5.4%; gephyrin, 49.4 ± 6.7%; *p = 0.012, *t* test; n = 4–5 neurons).

postembedding immuno-EM. We imaged cortical neurons immunolabeled with antibodies to cadherin-10 and either PSD-95 or gephyrin to label excitatory and inhibitory PSDs, respectively (Fig. 3A). SIM imaging revealed that cadherin-10 is organized into nanoscale subsynaptic puncta (Fig. 3A,B), rather than a single homogenous complex like PSD-95 or gephyrin. Additionally, cadherin-10 clusters were frequently distributed around the perimeter of the PSD-95 or gephyrin cluster, as demonstrated by line scans across the clusters (Fig. 3B). These features of cadherin-10 puncta contrast strikingly with line scans from lower-resolution conventional confocal images, which show cadherin-10 puncta to have similar sizes as PSD-95 clusters (Fig. 3C,D). In comparison, our SIM images show that cadherin-10 puncta have a mean diameter of 0.196 ± 0.003 μm (Fig. 3E), significantly smaller than either PSD-95 (0.409 ± 0.009 μm) or gephyrin (0.335 ± 0.008 μm; p = 0.0001, Kruskal–Wallis test; Fig. 3F–I) clusters. Although associated with both PSD-95 and gephyrin, cadherin-10 puncta displayed a preference for PSD-95-positive synapses; ~80% of PSD-95 clusters harbored cadherin-10 puncta compared with only ~51% of gephyrin clusters (*p = 0.012, t test; Fig. 3J). SIM, therefore, places cadherin-10 in synaptic nanoclusters that are associated with both excitatory and inhibitory PSDs.

Cadherin-10 is required for maintaining appropriate E/I synapse ratio in cortical neurons
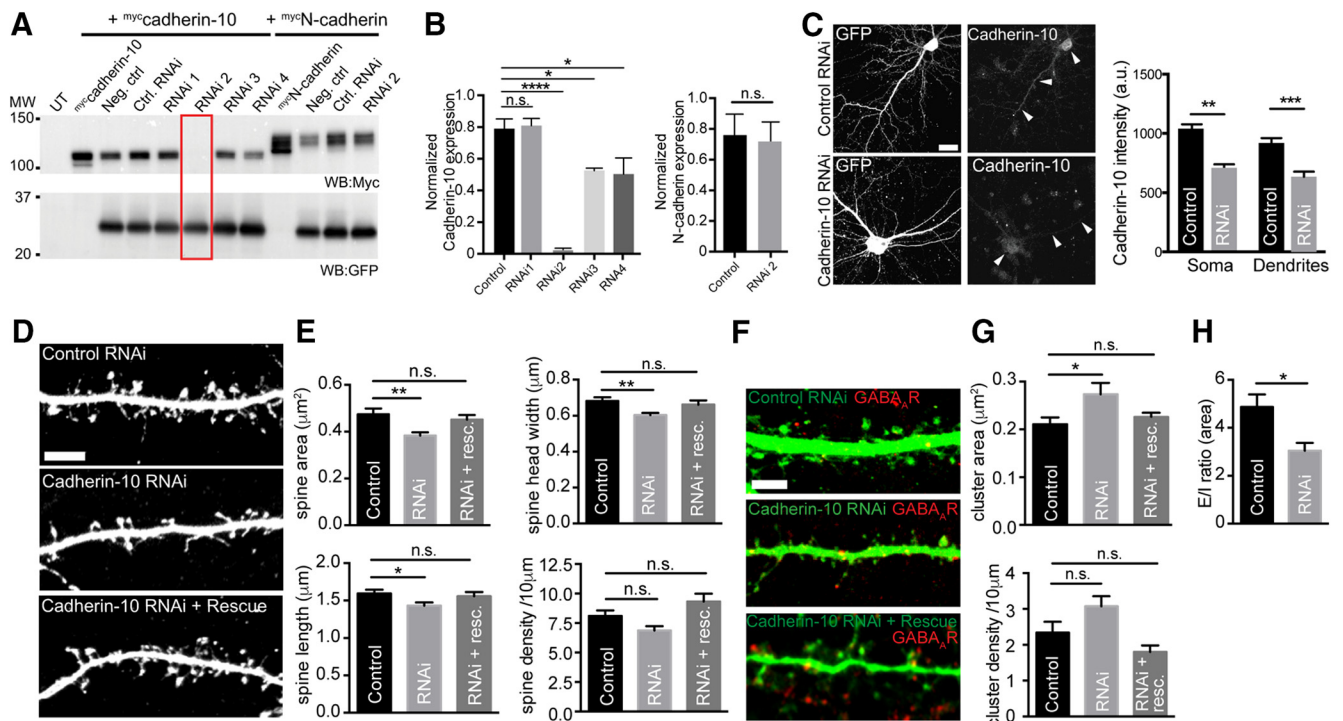
The presence of cadherin-10 puncta at both excitatory and inhibitory synapses suggests that they may play a role in maintaining synaptic structure at these sites. To test this hypothesis, we used RNAi to knock down cadherin-10. We tested four RNAi constructs in cadherin-10-expressing HEK293 cells (Fig. 4A,B), using the most effective (RNAi 2) in our experiments with cultured cortical neurons. This RNAi had no effect on N-cadherin expression levels (Fig. 4B) but effectively knocked down cadherin-10 in cortical neurons (Fig. 4C). DIV 21 cortical neurons were transfected with control and cadherin-10 constructs and fixed for subsequent analysis at DIV 24. Confocal imaging of control and cadherin-10 knock-down neurons and analysis of spine dimensions and density revealed a ~20% decrease in spine area (p = 0.0043, one-way ANOVA; Fig. 4D,E), reflecting a reduction in both spine width and length (Fig. 4E), and could be rescued by coexpression with RNAi-resistant cadherin-10 (Fig. 4E). There was a slight reduction in spine density with cadherin-10 RNAi that did not reach significance (Fig. 4D,E). Therefore, we conclude that cadherin-10 plays an important role in maintaining existing excitatory synapse structure.

We then analyzed inhibitory GABA$_A$ receptor (GABA$_A$R) clusters in control and knock-down neurons. Unexpectedly, we found that cadherin-10 knockdown caused a 22% increase in the GABA$_A$R cluster area (p = 0.0258, one-way ANOVA; Fig. 4F,G), which could be rescued by coexpression with RNAi-resistant cadherin-10, accompanied by a slight increase in cluster density that did not reach significance (p > 0.05, one-way ANOVA; Fig. 4F,G). As the areas of dendritic spines and synaptic GABA$_A$R clusters provide readouts of excitatory and inhibitory synaptic strength, respectively (Nusser et al., 1997; Sala and Segal, 2014), we calculated the ratio between spine and GABA$_A$R cluster areas in the same dendritic segment to compute an estimate of excitatory/inhibitory ratio per dendrite. This revealed that the ratio between excitatory and inhibitory synapse size was significantly reduced by ~40% in cadherin-10 knock-down neurons compared with controls (p = 0.010, t test; Fig. 4H).

Figure 4. Cadherin-10 knockdown reduces E/I synapse ratio in dendrites of cortical neurons *A*, Western blot (WB) analysis of lysates from HEK293 cells expressing ^{myc}cadherin-10 alone, or with GFP-expressing control or candidate RNAi constructs. The red box highlights effects of RNAi 2. *B*, Quantification of cadherin-10 RNAi knockdown in HEK293 cells. RNAi construct 2, which proved very effective, had no effect on N-cadherin expression and was used for all experiments (****$p < 0.0001$, 1-way ANOVA; $n = 3$ independent experiments). *C*, Maximum projections of confocal *z*-stacks showing cortical neurons expressing control or cadherin-10 RNAi and immunostained with antibodies to cadherin-10. Scale bar, 20 μm. Arrowheads point to cadherin-10 expression in soma and dendrites of neurons. Bar graphs show quantification of cadherin-10 in the soma and dendrites of control and knock-down neurons (**$p = 0.0019$; ***$p = 0.0009$; $n = 6 – 9$ neurons). *D*, Maximum projections of confocal *z*-stacks showing control, cadherin-10 knockdown, or knockdown and rescue expressing DIV 24 cortical neurons; neurons also express GFP to outline the dendrite. Scale bar, 5 μm. *E*, Quantification of spine area, width, length, and density (area, **$p = 0.0043$; width,**$p = 0.0037$; length,*$p = 0.0424$; density, $p > 0.05$; $n = 19 – 20$ neurons). *F*, Maximum projections of confocal *z*-stacks showing control, cadherin-10 knockdown, or knockdown and rescue of GFP-expressing DIV 24 cortical neurons (green) labeled with antibodies to α2-GABA$_A$R clusters (red). Scale bar, 5 μm. *G*. Quantification of α2-GABA$_A$R cluster area and density (area, *$p = 0.0258$; density, $p > 0.05$; $n = 17 – 23$ neurons). *H*, Quantification of ratio of spine area to GABA$_A$R cluster area in the same dendrite. The bar graph shows the E/I ratio is reduced from 4.9 $\pm$ 0.5 to 3.0 $\pm$ 1.3 in cadherin-10 knock-down neurons (E/I: *$p = 0.010$, $n = 10 – 12$ neurons).

Cadherin-10 is required for maintaining correct excitatory and inhibitory synaptic strength in cortical neurons

To determine whether these structural alterations were reflected by changes in synapse function, we then performed whole-cell electrophysiological recordings of mEPSCs and mIPSCs from control and cadherin-10 knock-down neurons (DIV 21 transfection, DIV 24 analysis; Fig. 5A). Consistent with our immunofluorescence data, cadherin-10 knockdown caused a reduction in mEPSC amplitude but an increase in mIPSC amplitude (mEPSCs, $p = 0.040$; mIPSCs, $p = 0.034$; t test; Fig. 5B,C). Importantly, neither mEPSC nor mIPSC frequency was significantly altered (Fig. 5D). Together with our imaging results (Fig. 4), these data indicate that cadherin-10 is required to maintain the proper ratio between the strength of excitatory and inhibitory synapses in dendrites of cortical neurons, without affecting their numbers.

Association of cadherin-10 with excitatory and inhibitory synaptic proteins

To elucidate mechanisms underlying the regulation of excitatory and inhibitory synapses by cadherin-10, we examined its interactions with major synapse type-specific molecules. Coimmunoprecipitations (coIPs) of cadherin-10 from cultured cortical lysates, followed by probing for interactions of synaptic proteins, revealed that cadherin-10 robustly participates in a complex with PSD-95 (Fig. 6A). We also observed a weak inter-

action between cadherin-10 and N-cadherin, suggesting that they may participate together in complexes at some synapses. However, we found no evidence of an association of cadherin-10 with multiple other adhesion molecules and neurotransmitter receptors. Cadherin-10 coIPs performed with rat cortical lysate demonstrated that cadherin-10 also associates with PSD-95 *in vivo*, suggesting this complex might be important for cadherin-10 function in the intact brain (Fig. 6B). Surprisingly, we did not detect coIP of the inhibitory scaffold gephyrin with cadherin-10 (Fig. 6A). However, the reverse coIP with gephyrin antibodies readily precipitated cadherin-10 (Fig. 6C), supporting the presence of cadherin-10 at inhibitory synapses in cortex. This result could be explained by the relative distributions of these proteins, assuming that a large proportion of gephyrin participates in complexes with cadherin-10 but a smaller fraction of cadherin-10 participates in complexes with gephyrin. To compare the relative synaptic distribution of N-cadherin and cadherin-10, we performed membrane fractionation experiments from mouse cortex, finding that N-cadherin is mainly associated with the membrane and PSD fractions (Fig. 6D), consistent with previous evidence that this type I cadherin is exclusively at excitatory PSDs (Benson and Tanaka, 1998). In contrast, cadherin-10 was present also in fractions containing membrane-associated proteins (usually associated with inhibitory synaptic components) as well as the PSD, supporting its presence at both synaptic sites.
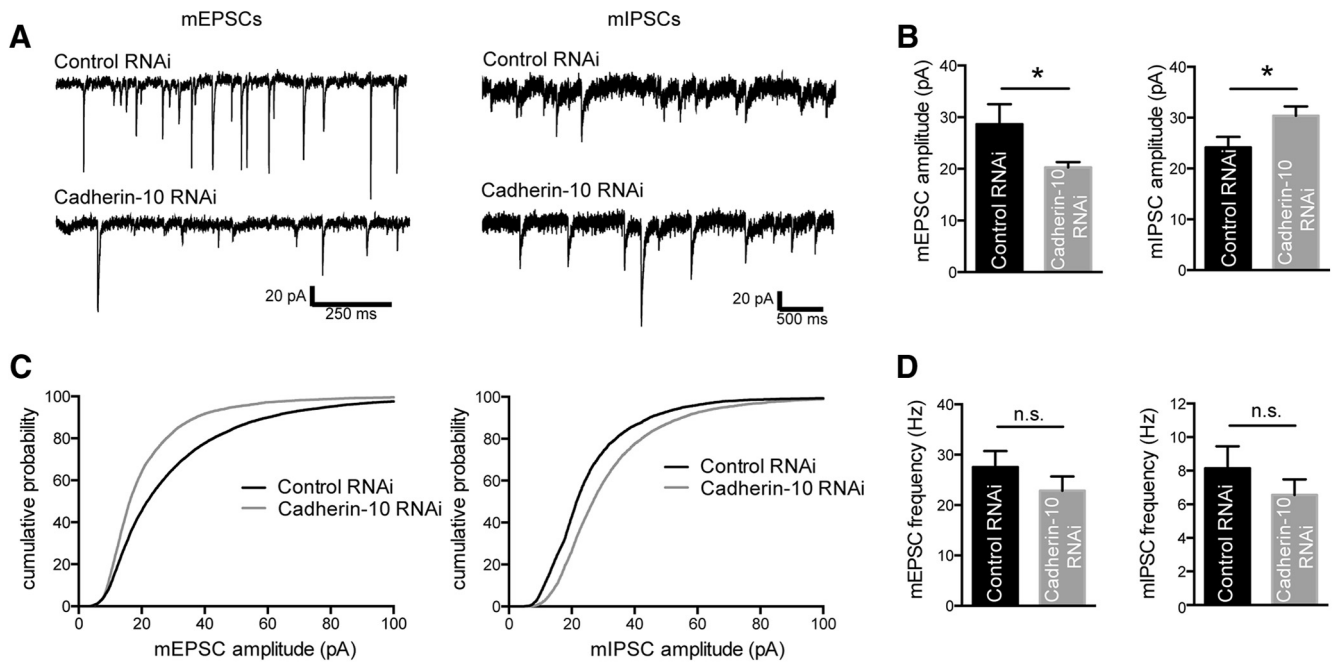
Figure 5. Cadherin-10 loss reciprocally modulates excitatory and inhibitory synaptic strength. *A*, Representative AMPA receptor-mediated mEPSC and GABA$_A$R-mediated mIPSC traces from control or cadherin-10 knock-down DIV 24 cortical neurons. *B*, Bar graphs of mEPSC and mIPSC amplitudes showing mEPSCs are reduced from 28.7 ± 3.8 pA to 20.3 ± 1.0 pA, and mIPSCs are increased from 24.0 ± 1.9 pA to 29.6 ± 1.7 pA (mEPSCs, *p = 0.040; mIPSCs, *p = 0.034; *t* tests; *n* = 14–15 neurons). *C*, Cumulative frequency graphs of mEPSC and mIPSC amplitudes. *D*, Bar graphs of mEPSC and mIPSC frequencies showing no significant difference (mEPSCs, *p* = 0.282; mIPSCs, *p* = 0.326; *t* tests; *n* = 12–13 neurons).

Nanoscale distribution of cadherin-10 puncta impacts synaptic scaffold dimensions

Analysis of SIM images of cadherin-10 and either PSD-95- or gephyrin-labeled neurons revealed that PSD-95 clusters harbored significantly larger numbers of cadherin-10 puncta compared with gephyrin clusters ($p < 0.0001$, Mann–Whitney test; Fig. 7A), even when normalized to the PSD cluster diameter ($p < 0.0001$, Mann–Whitney test; Fig. 7A), indicating that the larger number of cadherin-10 puncta at PSD-95-positive clusters is not only attributable to their larger size. We found that cadherin-10 puncta could be central (overlapping completely with the PSD), perisynaptic (contacting the edge of the PSD), or both central and perisynaptic (Fig. 7B). We categorized each PSD according to these three groups. The distribution patterns of cadherin-10 puncta were similar at PSD-95 and gephyrin PSDs ($p > 0.05$, two-way ANOVA; Fig. 7C). The majority of cadherin-10 puncta at both excitatory and inhibitory synapses were perisynaptic: only ∼10–20% of PSDs had either central puncta or a combination of central and perisynaptically positioned puncta. A significantly higher percentage of gephyrin clusters completely lacked cadherin-10 compared with PSD-95 clusters ($p < 0.001$, two-way ANOVA, Bonferroni's *post hoc* test; Fig. 7C). Comparing the diameters of PSDs with different cadherin-10 localization patterns revealed that PSD-95 and gephyrin clusters with both perisynaptic and centrally distributed cadherin-10 puncta were significantly larger than PSDs with no cadherin-10 or other distributions ($p = 0.0005$, $p = 0.0132$, one-way ANOVA; Fig. 7D). Thus, the nanoscale position of cadherin-10 puncta may be related to the size of the PSD at both excitatory and inhibitory synapses.

Our data show that cadherin-10 associates more robustly and displays more extensive colocalization with PSD-95 than gephyrin. We then asked whether cadherin-10 abundance was differentially related to the size of excitatory versus inhibitory synapses. We found a strong positive correlation between the number of

cadherin-10 puncta and the diameter of the associated PSD-95 cluster ($p < 0.0001$, Spearman's correlation; Fig. 7E,F) but a weaker correlation that did not reach significance between the number of cadherin-10 puncta and the size of gephyrin synapses ($p = 0.056$, Spearman's correlation; Fig. 7E,F). Likewise, the presence of cadherin-10 correlated with significantly larger PSD-95 clusters, but not with larger gephyrin clusters (PSD-95: $p = 0.015$, Mann–Whitney test; Fig. 7G), thereby reflecting potential differences in the association of cadherin-10 with PSD-95 compared with gephyrin. As cadherin-10 robustly interacts with PSD-95, and PSD-95 is essential for controlling the balance between excitatory and inhibitory synapses in dendrites (Levinson et al., 2010), we asked whether cadherin-10 knockdown altered the levels of PSD-95 in the neuron. Analysis of PSD-95 clusters in control and cadherin-10 knock-down neurons showed that both cluster density and total dendritic levels of PSD-95 were significantly reduced in cadherin-10 knock-down neurons ($p = 0.004$, *t* test; $p = 0.0354$, Mann–Whitney test; Fig. 7H,I), indicating that cadherin-10 may be required for maintaining the correct distribution and expression levels of PSD-95 in cortical dendrites.

Discussion

Type I classical cadherins are strongly implicated in many aspects of synaptic function (Hirano and Takeichi, 2012), but little is yet known about the differentially expressed type II cadherins and their functions in the brain. We find that the type II cadherin-10 is expressed at both excitatory and inhibitory synapses in cerebral cortex, where it regulates synapse structure and function, helping to control the balance between excitatory and inhibitory synaptic strength in cortical dendrites.

Cadherin-10 knockdown led to depression of excitatory synapses and concurrent enhanced strength of nearby inhibitory synapses, suggesting that it acts to maintain excitatory synaptic efficacy while constraining inhibitory synapse function. Interestingly, we
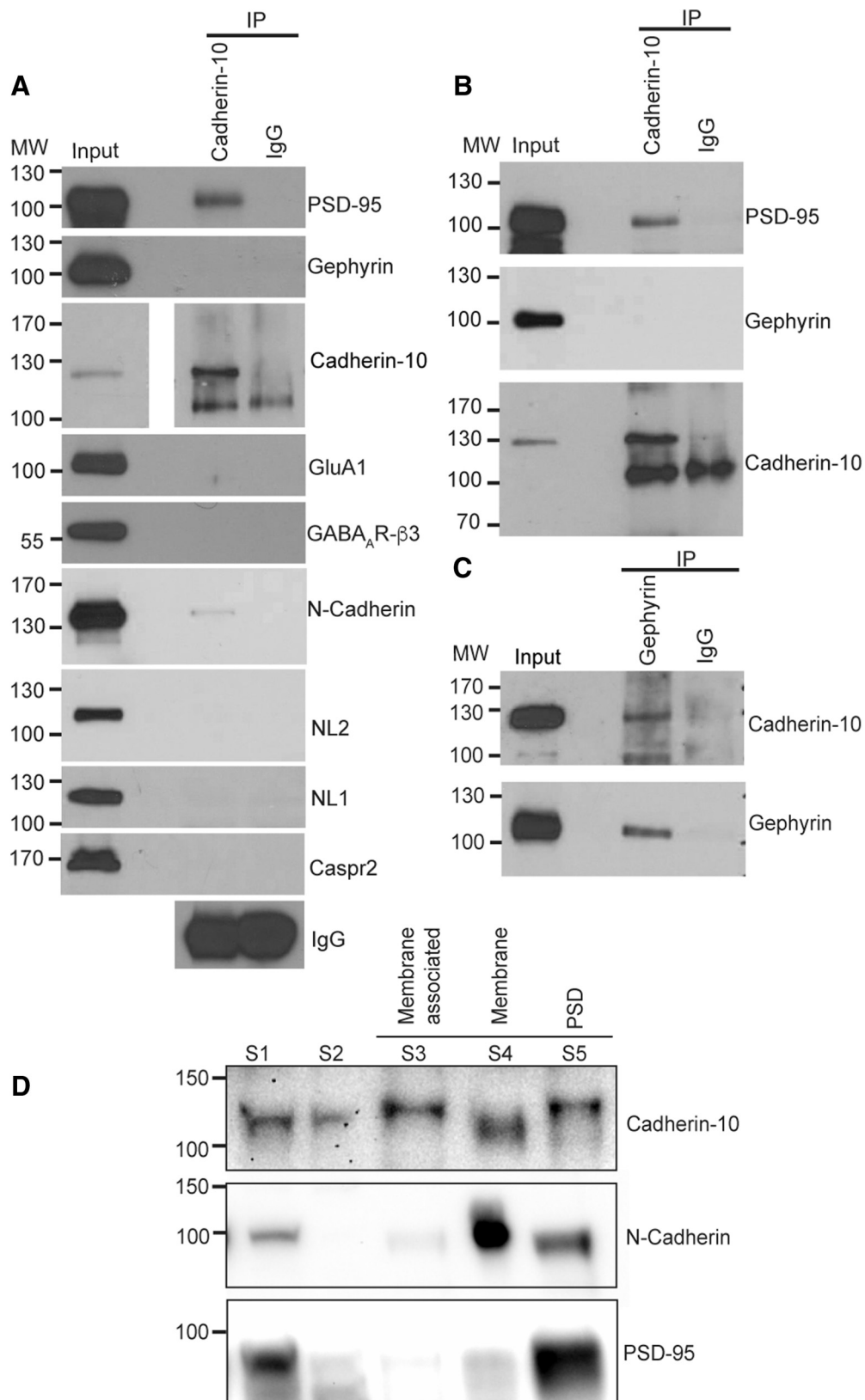
Figure 6. Cadherin-10 associates with PSD-95 and gephyrin **A**, Representative Western blot of cadherin-10 coIP from cultured cortical neurons (DIV 22) probed with synaptic proteins. A strong PSD-95 band and weak N-cadherin band are visible in the immunoprecipitation lane ($n = 4$ independent experiments). **B**, Representative Western blot of cadherin-10 coIP from rat cortical homogenate, showing interaction with PSD-95 but not gephyrin ($n = 3$ independent experiments). **C**, Representative Western blot of gephyrin coIP from rat cortical homogenate, showing interaction with cadherin-10 ($n = 3$ independent experiments). **D**, Representative Western blot of cortical membrane fractions. S1 and S2, crude homogenate; S3, membrane-associated protein; S5, membrane protein; S6, PSD protein. Cadherin-10 shows a strong band in the membrane-associated fraction, whereas a comparable band is barely visible for N-cadherin ($n = 3$ independent experiments). IP, Immunoprecipitation; MW, molecular weight.
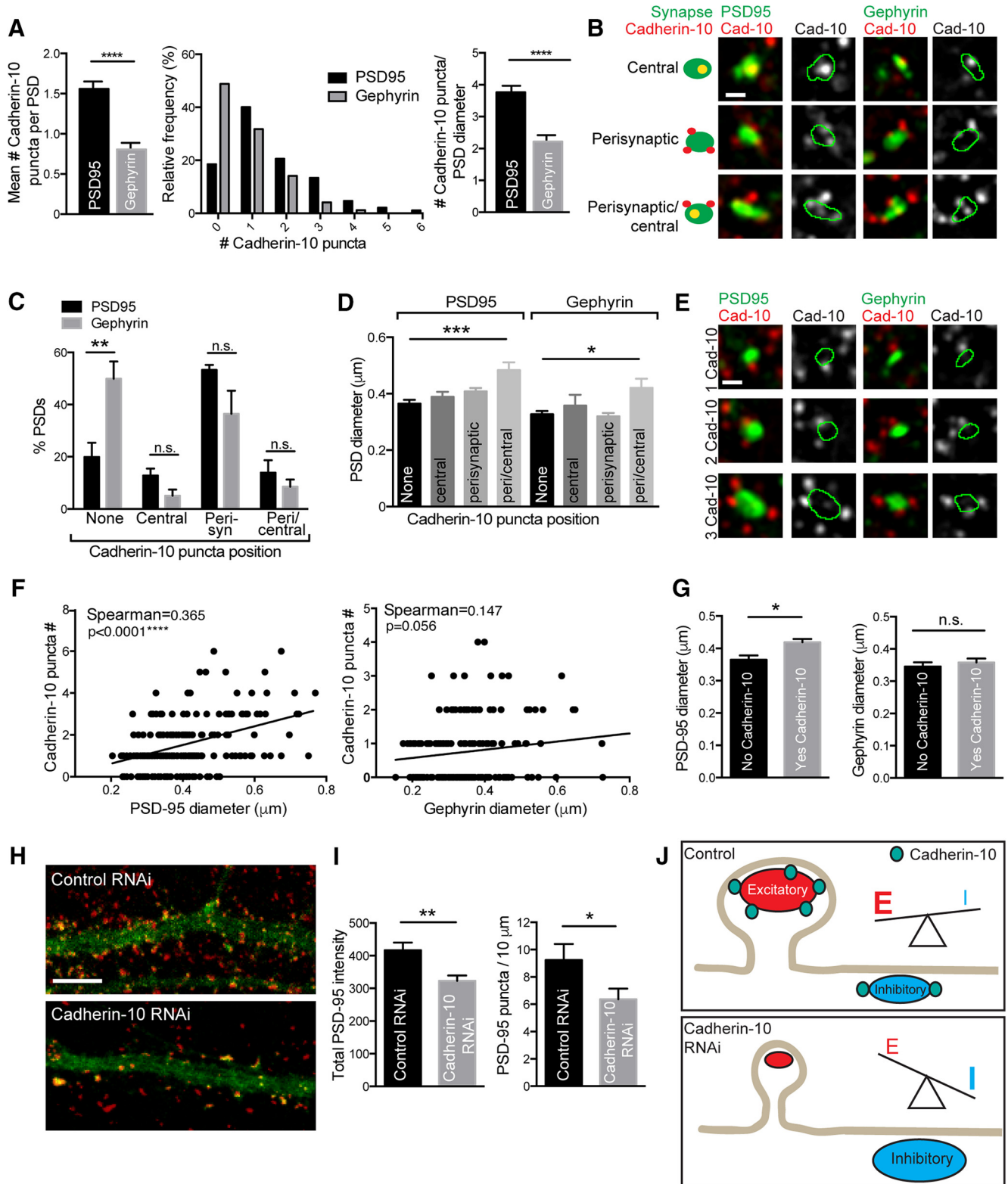
Figure 7. Nanoscale distribution of cadherin-10 puncta impacts synaptic scaffold dimensions ***A***, Mean number of cadherin-10 puncta per PSD-95- and gephyrin-positive synapse. Gephyrin PSDs have 50.6% fewer cadherin-10 puncta compared with PSD-95. Data are also shown as a frequency distribution histogram (****$p < 0.0001$, $n = 170–195$ PSDs). Right, cadherin-10 puncta number at PSD-95 and gephyrin PSDs, normalized to PSD diameter (****$p < 0.0001$, $n = 170–195$ PSDs). ***B***, SIM images show examples of different cadherin-10 puncta distributions. Scale bar, 0.2 μm; maximum projections of z-stacks. ***C***, Bar graphs showing percentage of PSD-95 and gephyrin synapses with different distributions of cadherin-10 puncta; the distribution of cadherin-10 puncta was similar at both PSDs (2-way ANOVA, $p > 0.05$; $n = 4–5$ neurons). Forty-nine percent of gephyrin PSDs had no cadherin-10 compared with 20% of PSD-95 PSDs (Bonferroni's *post hoc* test, **$p < 0.001$; $n = 4–5$ neurons). ***D***, PSD diameter correlates with subsynaptic distribution of cadherin-10 (***$p = 0.0005$; *$p = 0.0132$; 1-way ANOVA; $n = 170–195$ PSDs). ***E***. SIM images of different numbers of cadherin-10 puncta at PSD-95- and gephyrin-positive synapses. Scale bar, 0.2 μm; maximum projections of z-stack. ***F***, Correlation between PSD-95 or gephyrin diameter and number of cadherin-10 puncta ($n = 170–195$ PSDs, 4–5 neurons per condition). ***G***, Presence of cadherin-10 puncta correlates significantly with PSD-95 diameter but not gephyrin diameter (0.365 ± 0.01 μm to 0.419 ± 0.01 μm; PSD-95, *$p = 0.015$; gephyrin, $p = 0.197$; Mann–Whitney test; $n = 170–195$ PSDs; 4–5 neurons per condition). ***H***, Maximum (*Figure legend continues.*)

observed little effect of cadherin-10 manipulation on synapse number, suggesting that cadherin-10 regulates existing synapses, unlike other classical cadherins, which are thought to help control new synapse formation early in development (Brigidi and Bamji, 2011). Indeed, cadherins are often considered dispensable in mature neurons, where synapses are already established (Benson and Huntley, 2012), but our evidence that cadherin-10 helps to maintain the structure and strength of both excitatory and inhibitory synapses in mature cortical culture may be relevant also for other type II cadherins.

We show that cadherin-10 is present at presynaptic and postsynaptic sites of glutamatergic and GABAergic synapses, both *in situ* in layer 2/3 cortical neurons and in cortical culture, forming distinct nanoscale puncta considerably smaller than PSD-95 clusters. These puncta are small enough to contribute to the organization of the nanoscale scaffolding domains recently demonstrated by super-resolution microscopy for both excitatory and inhibitory PSD proteins (MacGillavry et al., 2013; Nair et al., 2013; Specht et al., 2013). We found that the size of PSD-95 clusters, but not of gephyrin clusters, strongly correlated with the number of associated cadherin-10 puncta, pointing to the importance of cadherin-10 for excitatory PSD integrity while suggesting that cadherin-10 may be less critical for inhibitory PSD integrity. We speculate that other adhesion molecules might help to maintain PSD structure at inhibitory synapses.

Cadherin-10 puncta occupied perisynaptic and central positions at both excitatory and inhibitory postsynaptic densities, which may be important for the structural organization of subsynaptic domains of the PSD and for the maintenance of overall stability. The position of subsynaptic cadherin-10 clusters at the PSD may be an important determinant of PSD size. Alternatively, there may be a "threshold" whereby above a certain concentration (perisynaptic and central positions) cadherin-10 supports a larger PSD. EM studies have shown that neuroligins are localized toward the center of the PSD (Mortillo et al., 2012), whereas N-cadherin is enriched at the outer rims of active zones and PSDs (Uchida et al., 1996). Furthermore, STED (stimulated emission depletion) imaging of hippocampal synapses has revealed that SynCAM1 is localized to the postsynaptic edges of the synaptic cleft, in contrast to EphB2, which lies further within the PSD (Perez de Arce et al., 2015). Interestingly, we find cadherin-10 is distributed both at the edge and in the center of the PSD. This places cadherin-10 puncta in a position where they may structurally contribute to the PSD of synapses.

Our data support a model whereby nanoscale subsynaptic cadherin-10 clusters regulate E/I balance by interacting with PSD proteins at both excitatory and inhibitory synapses (Fig. 7J). After knockdown of cadherin-10 in mature neurons, excitatory synapses are depressed with reduced spine area and depressed mEPSC amplitude, whereas inhibitory synapses within the same dendritic region display increased area and increased mIPSC amplitude. Knockdown of cadherin-10 also leads to fewer PSD-95 clusters and lower overall abundance of PSD-95 in dendrites, which may contribute to the E/I imbalance that we observe in these neurons. Our data suggest that several simultaneous processes may underlie the differential effects of cadherin-10 on excitatory and inhibitory synapses. First, cadherin-10 interacts differently with excitatory and inhibitory synapse stabilizing proteins, with possibly divergent consequences on the two types of synapses. Cadherin-10 interacts with PSD-95 and N-cadherin, which in turn help to maintain excitatory synapse structure and function. In contrast, at inhibitory synapses, cadherin-10 interacts with gephyrin, potentially with less affinity than with PSD-95, and does not complex with GABA$_A$Rs or neuroligins. Thus, the association of cadherin-10 with inhibitory synapses is likely weaker and poorly suited to promote synapse stabilization. In addition, we find higher expression of cadherin-10 at excitatory compared with inhibitory synapses, which could explain a stronger effect of cadherin-10 knockdown on excitatory synapses. In support of our finding, recent mass spectrometry proteomics reported a comparable distribution of cadherin-10 at excitatory versus inhibitory synapses in the mouse brain (excitatory, 26 peptides; inhibitory, 12 peptides; Loh et al., 2016).

Second, the interaction between cadherin-10 and PSD-95 may be important in governing the distribution of neuroligins between excitatory and inhibitory synapses, thereby controlling the E/I ratio. PSD-95 and cadherin-10 form complexes in cortex; this fact, along with our finding of a correlation between the number of cadherin-10 puncta and PSD-95 cluster dimensions, suggests that cadherin-10 may help to maintain the integrity and stability of PSD-95 clusters. PSD-95 is essential for maintaining synaptic specificity of neuroligin isoforms and controlling the balance between excitatory and inhibitory synapses within dendrites (Shipman et al., 2011). Reduced PSD-95 expression levels cause a redistribution of adhesion proteins from excitatory to inhibitory synapses, thereby altering the E/I balance in the dendrite (Graf et al., 2004; Prange et al., 2004; Levinson and El-Husseini, 2005; Gerrow et al., 2006; Levinson et al., 2010). Consistent with this model, our data suggest that cadherin-10 knockdown causes a reduction in overall PSD-95 expression, which could release other excitatory synaptic components (such as neuroligins) and allow their recruitment to inhibitory synapses within the same dendrite, thus promoting a shift in the E/I balance toward inhibition (Fig. 7J). Alternatively, cadherin-10 might exert a negative effect on synaptic gephyrin, perhaps by sequestering gephyrin to perisynaptic sites away from interactions with GABA$_A$Rs at the center of the synapse. On cadherin-10 knockdown this function would be relieved, thereby allowing inhibitory synapses to become larger. Further investigation will be required to assess this possibility.

A correct balance of excitation and inhibition is required for normal cortical function. Alterations in this balance in frontal regions are thought to contribute to neuropsychiatric disorders, including ASDs and schizophrenia (Gao and Penzes, 2015). Rare point mutations in genes encoding several other synaptic adhesion molecules, including neuroligins, neurexins, and other cadherins, have been detected in subjects with ASD (Betancur et al., 2009). Studies of these proteins point to synaptic pathways that can be disrupted in ASDs. However, since rare and highly penetrant mutations underlie only a small fraction of autism susceptibility ($<1\%$), it is also important to study the functions of common variants that likely work together to account for 50% of autism susceptibility (Gaugler et al., 2014). Here we describe the ASD common variant, cadherin-10, as a reciprocal regulator of excitatory and inhibitory synapses. We show here for the first

←

(*Figure legend continued.*) projections of confocal *z*-stacks showing PSD-95 (red) in control and cadherin-10 knock-down neurons. Scale bar, 5 μm. *I*, Total dendritic PSD-95 intensity and total cluster density in control and knock-down neurons. Both the total dendritic PSD-95 intensity and cluster density are reduced in knock-down neurons compared with control (total intensity: 416.9 ± 23.4 to $323 \pm 16.3.3$ mean gray values, **$p = 0.004$; density: 9.2 ± 1.2 to 6.4 ± 0.8 PSD-95 puncta/10 μm, *$p = 0.035$, Mann–Whitney tests; $n = 10$–11 neurons). *J*, Schematic diagram summarizes the effects of cadherin-10 knockdown on excitatory and inhibitory synapses. Cadherin-10 puncta are more abundant at excitatory synapses than inhibitory synapses. Cadherin-10 knockdown suppresses excitatory synaptic transmission and enhances inhibitory synaptic transmission, leading to a decrease in the dendritic E/I ratio.

time that a type II cadherin is localized to both excitatory and inhibitory synapses and controls their efficacy in opposite directions. Our data suggest that cadherin-10 contributes to the regulation of neuronal excitability in the cortex; dysregulation of this pathway may contribute to an abnormal excitatory/inhibitory balance that leads to psychiatric disorders.

References

Bekirov IH, Needleman LA, Zhang W, Benson DL (2002) Identification and localization of multiple classic cadherins in developing rat limbic system. Neuroscience 115:213–227. CrossRef Medline

Benson DL, Huntley GW (2012) Synapse adhesion: a dynamic equilibrium conferring stability and flexibility. Curr Opin Neurobiol 22:397–404. CrossRef Medline

Benson DL, Tanaka H (1998) N-cadherin redistribution during synaptogenesis in hippocampal neurons. J Neurosci 18:6892–6904. Medline

Betancur C, Sakurai T, Buxbaum JD (2009) The emerging role of synaptic cell-adhesion pathways in the pathogenesis of autism spectrum disorders. Trends Neurosci 32:402–412. CrossRef Medline

Brigidi GS, Bamji SX (2011) Cadherin-catenin adhesion complexes at the synapse. Curr Opin Neurobiol 21:208–214. CrossRef Medline

Connolly JJ, Glessner JT, Hakonarson H (2013) A genome-wide association study of autism incorporating autism diagnostic interview-revised, autism diagnostic observation schedule, and social responsiveness scale. Child Dev 84:17–33. CrossRef Medline

Duan X, Krishnaswamy A, De la Huerta I, Sanes JR (2014) Type II cadherins guide assembly of a direction-selective retinal circuit. Cell 158:793–807. CrossRef Medline

Frost NA, Shroff H, Kong H, Betzig E, Blanpied TA (2010) Single-molecule discrimination of discrete perisynaptic and distributed sites of actin filament assembly within dendritic spines. Neuron 67:86–99. CrossRef Medline

Gao R, Penzes P (2015) Common mechanisms of excitatory and inhibitory imbalance in schizophrenia and autism spectrum disorders. Curr Mol Med 15:146–167. CrossRef Medline

Gaugler T, Klei L, Sanders SJ, Bodea CA, Goldberg AP, Lee AB, Mahajan M, Manaa D, Pawitan Y, Reichert J, Ripke S, Sandin S, Sklar P, Svantesson O, Reichenberg A, Hultman CM, Devlin B, Roeder K, Buxbaum JD (2014) Most genetic risk for autism resides with common variation. Nat Genet 46:881–885. CrossRef Medline

Gerrow K, Romorini S, Nabi SM, Colicos MA, Sala C, El-Husseini A (2006) A preformed complex of postsynaptic proteins is involved in excitatory synapse development. Neuron 49:547–562. CrossRef Medline

Gil OD, Needleman L, Huntley GW (2002) Developmental patterns of cadherin expression and localization in relation to compartmentalized thalamocortical terminations in rat barrel cortex. J Comp Neurol 453:372–388. CrossRef Medline

Graf ER, Zhang X, Jin SX, Linhoff MW, Craig AM (2004) Neurexins induce differentiation of GABA and glutamate postsynaptic specializations via neuroligins. Cell 119:1013–1026. CrossRef Medline

Gustafsson MG (2005) Nonlinear structured-illumination microscopy: wide-field fluorescence imaging with theoretically unlimited resolution. Proc Natl Acad Sci U S A 102:13081–13086. CrossRef Medline

Hirano S, Takeichi M (2012) Cadherins in brain morphogenesis and wiring. Physiol Rev 92:597–634. CrossRef Medline

Klei L, Sanders SJ, Murtha MT, Hus V, Lowe JK, Willsey AJ, Moreno-De-Luca D, Yu TW, Fombonne E, Geschwind D, Grice DE, Ledbetter DH, Lord C, Mane SM, Martin CL, Martin DM, Morrow EM, Walsh CA, Melhem NM, Chaste P, et al. (2012) Common genetic variants, acting additively, are a major source of risk for autism. Mol Autism 3:9. CrossRef Medline

Kuwako K, Nishimoto Y, Kawase S, Okano HJ, Okano H (2014) Cadherin-7 regulates mossy fiber connectivity in the cerebellum. Cell Rep 9:311–323. CrossRef Medline

Levinson JN, El-Husseini A (2005) New players tip the scales in the balance between excitatory and inhibitory synapses. Mol Pain 1:12. CrossRef Medline

Levinson JN, Li R, Kang R, Moukhles H, El-Husseini A, Bamji SX (2010) Postsynaptic scaffolding molecules modulate the localization of neuroligins. Neuroscience 165:782–793. CrossRef Medline

Loh KH, Stawski PS, Draycott AS, Udeshi ND, Lehrman EK, Wilton DK, Svinkina T, Deerinck TJ, Ellisman MH, Stevens B, Carr SA, Ting AY, et al (2016) Proteomic analysis of unbounded cellular compartments: synaptic clefts. Cell 166:1295–1307. CrossRef Medline

Lu HE, MacGillavry HD, Frost NA, Blanpied TA (2014) Multiple spatial and kinetic subpopulations of CaMKII in spines and dendrites as resolved by single-molecule tracking PALM. J Neurosci 34:7600–7610. CrossRef Medline

Ma D, Salyakina D, Jaworski JM, Konidari I, Whitehead PL, Andersen AN, Hoffman JD, Slifer SH, Hedges DJ, Cukier HN, Griswold AJ, McCauley JL, Beecham GW, Wright HH, Abramson RK, Martin ER, Hussman JP, Gilbert JR, Cuccaro ML, Haines JL, et al. (2009) A genome-wide association study of autism reveals a common novel risk locus at 5p14.1. Ann Hum Genet 73:263–273. CrossRef Medline

MacGillavry HD, Song Y, Raghavachari S, Blanpied TA (2013) Nanoscale scaffolding domains within the postsynaptic density concentrate synaptic AMPA receptors. Neuron 78:615–622. CrossRef Medline

Mortillo S, Elste A, Ge Y, Patil SB, Hsiao K, Huntley GW, Davis RL, Benson DL (2012) Compensatory redistribution of neuroligins and N-cadherin following deletion of synaptic beta1-integrin. J Comp Neurol 520:2041–2052. CrossRef Medline

Nair D, Hosy E, Petersen JD, Constals A, Giannone G, Choquet D, Sibarita JB (2013) Super-resolution imaging reveals that AMPA receptors inside synapses are dynamically organized in nanodomains regulated by PSD95. J Neurosci 33:13204–13224. CrossRef Medline

Nusser Z, Cull-Candy S, Farrant M (1997) Differences in synaptic GABA(A) receptor number underlie variation in GABA mini amplitude. Neuron 19:697–709. CrossRef Medline

Perez de Arce K, Schrod N, Metzbower SW, Allgeyer E, Kong GK, Tang AH, Krupp AJ, Stein V, Liu X, Bewersdorf J, Blanpied TA, Lucić V, Biederer T (2015) Topographic mapping of the synaptic cleft into adhesive nanodomains. Neuron 88:1165–1172. CrossRef Medline

Prandini P, Pasquali A, Malerba G, Marostica A, Zusi C, Xumerle L, Muglia P, Da Ros L, Ratti E, Trabetti E, Pignatti PF (2012) The association of rs4307059 and rs35678 markers with autism spectrum disorders is replicated in Italian families. Psychiatr Genet 22:177–181. CrossRef Medline

Prange O, Wong TP, Gerrow K, Wang YT, El-Husseini A (2004) A balance between excitatory and inhibitory synapses is controlled by PSD-95 and neuroligin. Proc Natl Acad Sci U S A 101:13915–13920. CrossRef Medline

Sala C, Segal M (2014) Dendritic spines: the locus of structural and functional plasticity. Physiol Rev 94:141–188. CrossRef Medline

Shimoyama Y, Tsujimoto G, Kitajima M, Natori M (2000) Identification of three human type-II classic cadherins and frequent heterophilic interactions between different subclasses of type-II classic cadherins. Biochem J 349:159–167. CrossRef Medline

Shipman SL, Schnell E, Hirai T, Chen BS, Roche KW, Nicoll RA (2011) Functional dependence of neuroligin on a new non-PDZ intracellular domain. Nat Neurosci 14:718–726. CrossRef Medline

Smith KR, Kopeikina KJ, Fawcett-Patel JM, Leaderbrand K, Gao R, Schürmann B, Myczek K, Radulovic J, Swanson GT, Penzes P (2014) Psychiatric risk factor ANK3/ankyrin-G nanodomains regulate the structure and function of glutamatergic synapses. Neuron 84:399–415. CrossRef Medline

Specht CG, Izeddin I, Rodriguez PC, El Beheiry M, Rostaing P, Darzacq X, Dahan M, Triller A (2013) Quantitative nanoscopy of inhibitory synapses: counting gephyrin molecules and receptor binding sites. Neuron 79:308–321. CrossRef Medline

Suzuki SC, Inoue T, Kimura Y, Tanaka T, Takeichi M (1997) Neuronal circuits are subdivided by differential expression of type-II classic cadherins in postnatal mouse brains. Mol Cell Neurosci 9:433–447. CrossRef Medline

Uchida N, Honjo Y, Johnson KR, Wheelock MJ, Takeichi M (1996) The catenin/cadherin adhesion system is localized in synaptic junctions bordering transmitter release zones. J Cell Biol 135:767–779. CrossRef Medline

Wang K, Zhang H, Ma D, Bucan M, Glessner JT, Abrahams BS, Salyakina D, Imielinski M, Bradfield JP, Sleiman PM, Kim CE, Hou C, Frackelton E, Chiavacci R, Takahashi N, Sakurai T, Rappaport E, Lajonchere CM, Munson J, Estes A, et al. (2009) Common genetic variants on 5p14.1 associate with autism spectrum disorders. Nature 459:528–533. CrossRef Medline

Williams ME, Wilke SA, Daggett A, Davis E, Otto S, Ravi D, Ripley B, Bushong EA, Ellisman MH, Klein G, Ghosh A (2011) Cadherin-9 regulates synapse-specific differentiation in the developing hippocampus. Neuron 71:640–655. CrossRef Medline